Powering of an HTS Dipole Insert-Magnet Operated Standalone in Helium Gas between 5 and 85 K

J. van Nugteren[1], G. Kirby[1], H. Bajas[1], M. Bajko[1], A. Ballarino[1], L. Bottura[1], A. Chiuchiolo[1], P-A. Contat[1], M. Dhallé[2], M. Durante[3], P. Fazilleau[3], A. Fontalva[1], P. Gao[2], W. Goldacker[4], H. ten Kate[1], A. Kario[4], V. Lahtinen[5], C. Lorin[3], A. Markelov[6], J. Mazet[1], A. Molodyk[6], J. Murtomäki[1], N. Long[7], J. Perez[1], C. Petrone[1], F. Pincot[1], G. de Rijk[1], L. Rossi[1], S. Russenschuck[1], J. Ruuskanen[5], K. Schmitz[1], A. Stenvall[5], A. Usoskin[8], G. Willering[1] and Y. Yang[9]

[1] CERN, CH-1211 Geneva 23, Geneva, Switzerland
[2] University of Twente, Drienerlolaan 5, 7522NB Enschede, Netherlands
[3] CEA Saclay, Gif-sur-Yvette 91191, Cedex, France
[4] Karlsruhe Institute of Technology, 76131 Karlsruhe, Germany
[5] Tampere University of Technology, Korkeakoulunkatu 10, 33720 Tampere, Finland
[6] SuperOx, 20/2 Nauchnyi proezd, 117246 Moscow, Russia
[7] Victoria University of Wellington, PO Box 600 Wellington 6140, New Zealand
[8] Bruker HTS, Ehrichstraße 10, 63450 Hanau, Germany
[9] University of Southampton, University Road, Southampton SO17 1BJ, UK

E-mail: `jeroen.van.nugteren@cern.ch`

January 2018

Abstract. This paper describes the standalone magnet cold testing of the high temperature superconducting magnet Feather-M2.1-2. This magnet was constructed within the European funded FP7-EUCARD2 collaboration to test Roebel type HTS cable, and is one of the first high temperature superconducting dipole magnets in the world. The magnet was operated in forced flow helium gas with temperatures ranging between 5 to 85 K. During the tests a magnetic dipole field of 3.1 T was reached inside the aperture at a current of 6.5 kA and a temperature of 5.7 K. These values are in agreement with the self-field critical current of the used SuperOx cable assembled with Sunam tapes (low-performance batch), thereby confirming that no degradation occurred during winding, impregnation, assembly and cool-down of the magnet. The magnet was quenched many tens of times by ramping over the critical current and no degradation nor training was evident. During the tests the voltage over the coil was monitored in the micro-volt range. An inductive cancellation wire was used to remove the inductive component, thereby significantly reducing noise levels. Close to the quench current, drift was detected both in temperature and voltage over the coil. This drifting happens in a time scale of minutes and is a clear indication that the magnet has reached its limit. All quenches happened approximately at the same average electric field and thus none of the quenches occurred unexpectedly.

Keywords: Superconducting Magnets, Superconducting Accelerator Magnets, High-Temperature Superconductors (HTS), Testing Submitted to: *Supercond. Sci. Technol.*

1. Introduction

Feather-M2 is an HTS accelerator dipole insert-magnet designed and constructed in the framework of EUCARD2 WP10.3 [1,2], which serves as a test of HTS conductor being part of a magnet. The magnet was designed to generate the required 5 T central magnetic field when operated in standalone, while maximizing the magnetic field contribution when operated inside a background field, for example supplied by the 13-15 T Fresca2 magnet [3–5]. To this purpose a novel layout type named Aligned Block is used [6, 7]. In this layout the HTS superconducting tapes are aligned with the magnetic field lines when the magnet is operated as insert inside a background magnetic field. This results in 2-5 times higher engineering current densities, compared to the unaligned case [8], but should also reduce screening current effects, thereby improving magnetic field quality.

At present (Summer 2017) the first two magnet poles named Feather-M2.1 and Feather-M2.2 have been wound, impregnated and assembled with Roebel cable [9–13], cabled by SuperOx [14] using ReBCO coated conductor tape from Sunam [15], following the punch-and-coat route. This cable has a much lower (factor 3 [16]) engineering current density than the final cable of the EuCARD2 program, whose tape has been manufactured by Bruker HTS [17] and has been assembled into Roebel cable by KIT [18]. This last cable was not available at the time of winding and will be tested in a magnet called Feather-M2.3-4 as a next step. Due to the low performance of the SuperOx/Sunam cable, the initial set of poles should be considered as practice coils in order to eliminate potential issues before using the more costly high performance cable. Winding of this cable onto the Feather-M2.3 and Feather-M2.4 poles is now foreseen early 2018.

After assembly of the two poles, the Feather-M2.1-2 magnet was tested standalone inside an iron yoke. Similar to the sub-scale prototype racetrack coil Feather-M0.4, tested last year at CERN [19], the magnet is operated inside forced flow Helium gas with variable temperature. Despite the low performance of the cable, the cold powering tests offer valuable insight into the future use of HTS inside accelerator magnets, like FCC [20, 21]. This paper briefly presents the assembly of the Feather-M2.1-2 (SuperOx, Sunam) magnet, the results from the first cold powering test and the insights gained. For convenience, the specifications of the Feather-M2.1-2 magnet and SuperOx/Sunam cable are summarized in Tables 1 and 2, respectively. The definition of the used parameters is provided in respective Figures 1 and 2. After the initial series of tests presented in this paper, a set of Hall probes and pick-up coils were installed in the magnet's aperture in order to perform magnetic measurements. The results of these additional tests, showing dynamic field effects, are published separately in [22].

Table 1. Geometric specifications of the Feather-M2.1-2 magnet. The used parameters are clarified in Figure 1. Table adapted from [7,8].

Symbol	Value	Description
ϕ_{in}	40.0 mm	aperture diameter
ϕ_{out}	99.0 mm	outer diameter
d_{ap}	2.0 mm	extra aperture spacing
R_{yoke1}	51.0 mm	yoke inner radius
R_{yoke2}	111.0 mm	yoke outer radius
L_{yoke}	800.0 mm	yoke length
n_{turn1}	8	central deck number of turns
n_{turn2}	4	wing deck number of turns
L_0	100.0 mm	straight section length
L_{w}	44.0 mm	straight section width
L_{co}	720 mm	total coil length
y_{cen1}	3.8 mm	central deck y-position
y_{cen2}	17.3 mm	wing deck y-position
h_{end1}	21.3 mm	central deck flaring height
h_{end2}	21.3 mm	wing deck flaring height
a_{end}	4.0 degree	flaring angle at coil end
a_{rot1}	0.5 degree	central shear angle
a_{rot2}	8.0 degree	wing shear angle
p_{twist}	0.6	shear angle factor
R_{easy}	16.0 mm	easy-way bend radius
R_{mid}	400 mm	mid-coil bend radius
R_{hard}	2000 mm	hard-way bend radius
ℓ_{cen}	12.2 m	central deck cable length
ℓ_{wing}	3.6 m	wing deck cable length
ℓ_{lead}	1.35 m	length of each current lead
ℓ_{pole}	18.5 m	cable length in each pole
ℓ_{total}	37 m	total cable length in magnet
L_{self}	166 μH	magnet self-inductance
E_{stored}	2.9 kJ	stored energy at 6 kA/3 T

Table 2. Geometric specifications of the used Roebel cable used in Feather-M2.1-2, assembled by SuperOx from Sunam tape. The used parameters are clarified in Figure 2. Table adapted from [7,8].

Symbol	Value	Description
N_{s}	15	number of tapes
d_{s}	0.15 mm	tape thickness
d_{c}	1.2 mm	cable total thickness
d_{i}	0.1 mm	insulation thickness
W_{r}	5.00 mm	tape width
W_{t}	12.0 mm	cable width
W_{x}	6.00 mm	cross over width
W_{c}	2.0 mm	channel width
Φ	30 degree	cross over angle
L_{tp}	300 mm	transposition pitch
r_{i}	6.0 mm	inner radius
r_{o}	0.0 mm	outer radius

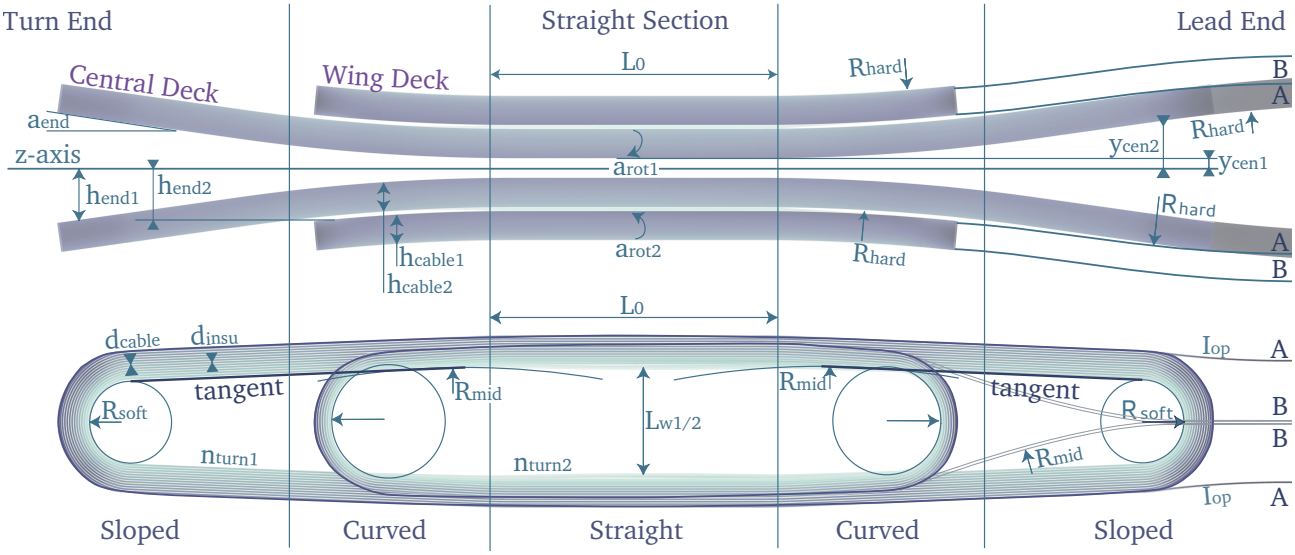

Figure 1. Side and top views on the geometry of the Feather-M2 coil and the definition of its geometric parameters. Respective values of the magnet tested are presented in Table 1. Note that the illustration is not to scale. Illustration adapted from [7, 8].

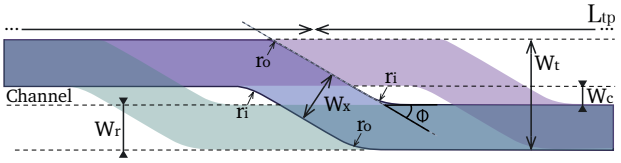

Figure 2. Definition of parameters for the geometry of a Roebel cable [23]. Respective values can be found in Table 2. Illustration adapted from [7, 8].

2. Winding, Impregnation and Assembly

One of the important findings of EUCARD2 is that the classical fiber-glass epoxy insulation and impregnation scheme can also be applied to HTS. To avoid high stresses due to the Lorentz forces on the complex cable geometry [24] it is necessary to fill all voids with epoxy resin. The resin spreads out the stresses and avoids scissoring and peel-off effects of the tapes along the edges at the cross-over locations.

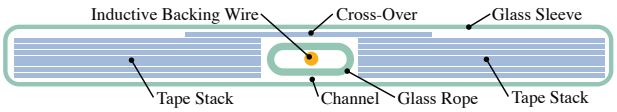

Figure 3. Illustration showing the cross-section of a Roebel cable, its nomenclature and the used insulation scheme.

To avoid delamination [25] of the tapes, it is important that the thermal contraction of the epoxy matches that of the tapes [26]. Therefore it was decided to use clear epoxy resin (CTD101K [27]) in combination with glass fibers (see Figure 3). These glass fibers comprise of a rope inside the channel at the center of the cable and a sleeve on the outside, which is also part of the turn-to-turn insulation. The resulting glass-fiber epoxy has about the same thermal contraction as copper and stainless steel. The resin was cured using the standard cycle of 5 hours at 110 °C then 16 hour at 125 °C. Using this scheme it was experimentally determined, by the University of Twente, that the coil pack can resist a transverse pressure exceeding 400 MPa [28, 29]. To avoid the impregnated coil pack being under tension, another suspected cause for delamination, it was decided to mould-release the central former. During the winding and impregnation the coil pack is put under a slight compression of 2 to 5 MPa in order to achieve good electrical contact between all the tapes. This is necessary to improve the thermal stability of the coil and to allow current sharing between the tapes in case of small defects.

Figure 4 shows a rendering of the parts making up one magnet pole of the Feather-M2 magnet. The Roebel cable is wound onto a central former, as shown in Figure 5. The cable is surrounded by a set of spacers, allowing the OFHC copper Inductively Coupled Energy Dissipation (ICED) rings [30–33] to be inserted from the top. A set of G11 sheets electrically insulate the decks from one another and from ground. Iron pole pieces are inserted to increase the magnetic field by another 0.4 T. The forces onto the end of the coil are intercepted by a set of stainless steel end-plates. Each pole of the magnet is wound on top of the impregnation mould, which when closed is by itself vacuum tight. This allows for impregnation without using a vacuum chamber. The impregnated coils, shown in Figure 6, are assembled together inside an

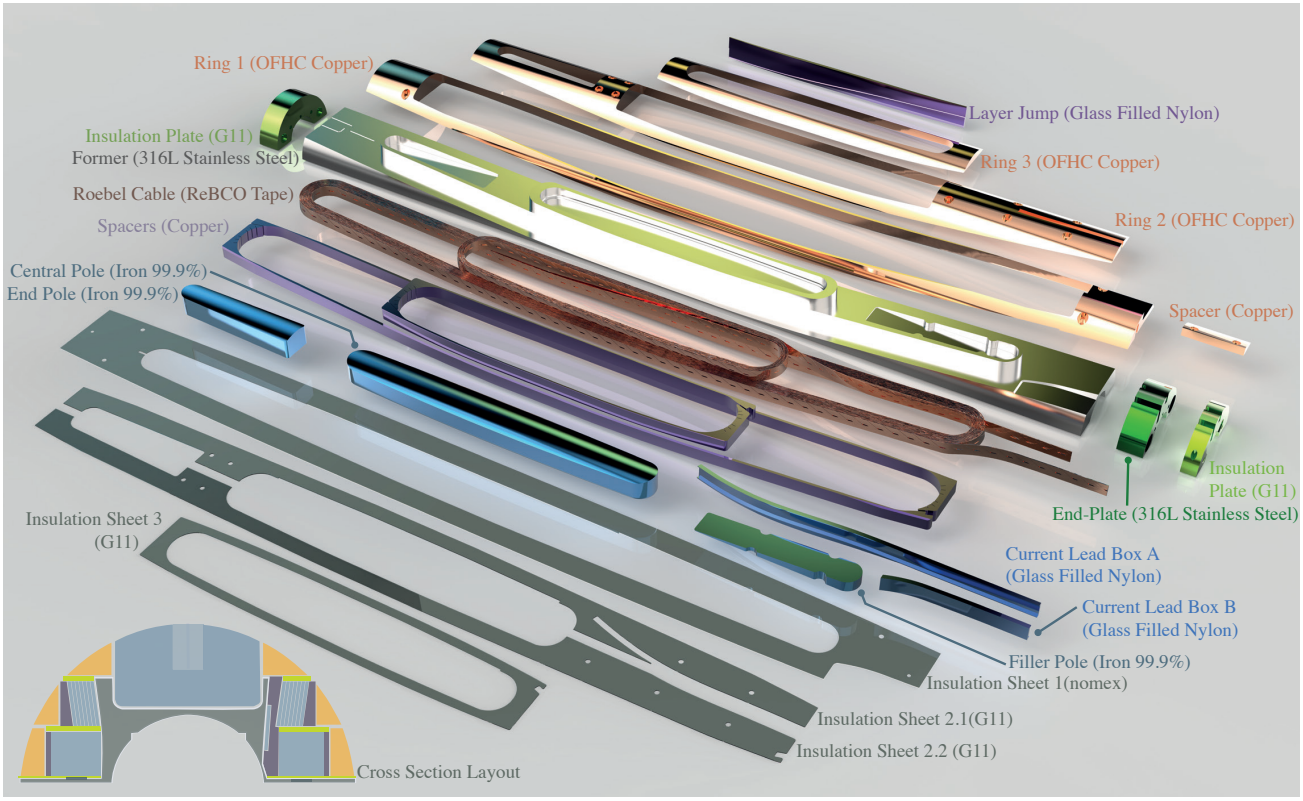

Figure 4. Rendering showing an exploded view of all the parts making up one of the Feather-M2 magnet poles. Visible from top to bottom are the copper rings, the spacers, the coil-windings and joint area, the former, the iron poles and the G11 insulation sheets.

aluminum cylinder, which is responsible for containing the radial forces. The iron yoke was assembled around the magnet after which the current lead connections are made.

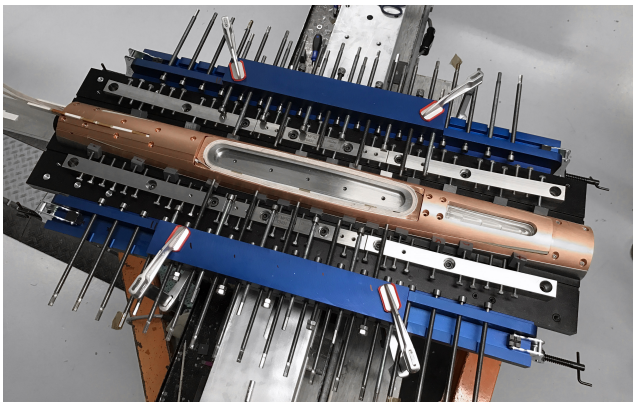

Figure 5. Photograph showing an overview of Feather-M2.1 during coil winding. Visible are the individual turns, the copper spacer and ring, the former and the winding and impregnation tooling.

The resistances between coil, ground and instrumentation are in all cases in the range of 100 GΩ indicating that the used impregnation and insulation system is adequate. In addition a fast discharge test was performed, up to 2 kV, to check for turn-to-turn shorts. It was observed that the voltage recordings were similar between Feather-M2.1 and Feather-M2.2 for all amplitudes and thus no shorts were revealed.

3. Instrumentation and Noise Levels

Because quench detection and protection was a major concern, Feather-M2.1-2 features some instrumentation that is not very common for accelerator magnets. A simplified wiring diagram providing an overview of the instrumentation on the coils is shown in Figure 7. Visible are the two main current leads A and B, part of the test facility, with the two coils, Feather-M2.1 and Feather-M2.2 connected via an interlayer splice. Each of the leads, exiting the coils, has two voltage taps (for redundancy), forming a twisted pair with the wire of the opposing lead. The voltage taps are soldered to an arbitrary tape in the cable, which is not necessarily the same one on either side of the coil. Each lead is also equipped with a set of pick-up coils to measure fast changes of the current distribution between the tapes inside the cable. A temperature sensor is mounted inside the copper ring both on the lead-end and turn-end of each coil. These temperature sensors are used to determine the operating temperature of the magnet. Ad-

Figure 6. Feather-M2.1-2 poles before applying the polyimide insulation sheet and insertion into its aluminum support cylinder.

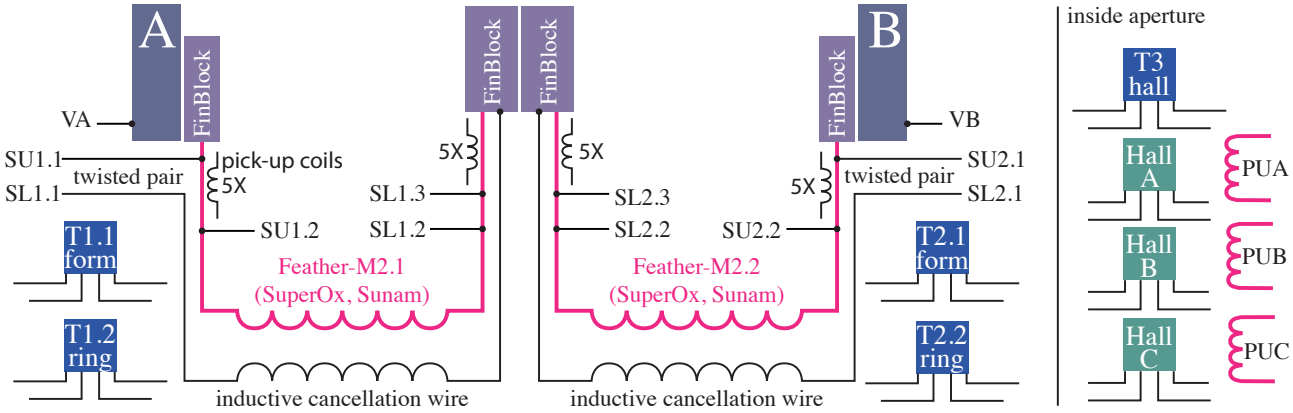

Figure 7. Simplified wiring diagram illustrating the instrumentation used in the Feather-M2.1-2 magnet.

ditional temperature sensors are present on the main current leads and outside of the yoke. Inside the aperture a set of three Hall probes is present, each of which is backed by a pick-up coil to ensure proper calibration, as the used Hall probes are not stable during the variable temperature operation.

In order to measure only the resistive component of the voltage over the coils and greatly reduce the noise-to-signal ratio of the voltage taps, an inductive backing wire [34] was inserted inside the central channel of the used Roebel cable (see Figures 3 and 8). This enamel coated copper wire follows exactly the same path as the cable and thus the induced voltage over it is the same. This voltage is then subtracted from the measured voltage over coil. The noise level measured is about one-third of the noise level of the differential signal between the two poles of the magnet, not using the subtraction from the inductive wire. Also as intended it contains a near zero inductive component making data analysis and EI-curve (average electric field, generated by the resistive transition, against current, see Section 6) fitting much easier, thereby providing a useful tool for analysis. The measured noise level in the voltage signal of each pole, at a sampling frequency of about 3 Hz, is approximately 2 μV, equaling an electric field of 0.1 μV/m.

In addition to the temperature sensors, also optical fibers with Bragg gratings [35, 36], a relatively new temperature monitoring technique, were used on

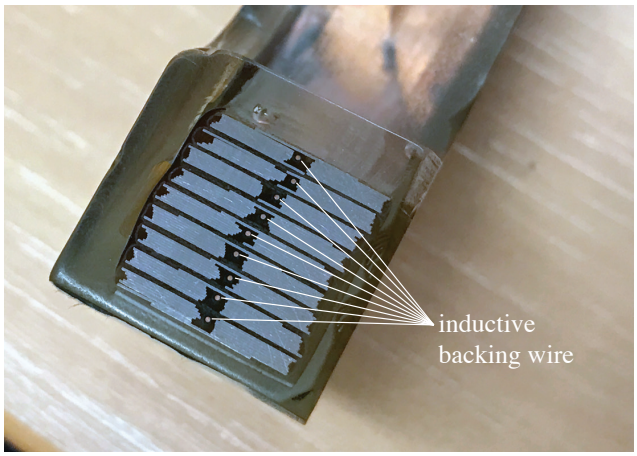

Figure 8. A cross section of the impregnated coil pack with dummy Roebel cable. Visible is the inductive backing wire at the center of the cable.

the outside of the coil to map the temperature of important components, such as the joints and the top of the coil. The temperature as measured by the optical fibers was in good agreement with the classical temperature sensors, showing that the system is working correctly. For the next Feather-M2.3-4 coil it is planned to integrate these fibers inside the G11 insulation sheets to allow monitoring of local cable temperature rises during drift (see Section 7).

4. Cool-down, Critical Temperature and Triple-R

The RRR (Residual Resistivity Ratio) of the copper stabilizer reflects the purity and hardness state of the copper and is important to determine stability, losses and quench behavior of the magnets. Because of this, it is as well an important input parameter for numerical models, to study, for example, quenches in HTS coils. The RRR is defined as the resistivity of the copper at 273 K divided with its resistivity at 10 K. To determine the RRR, the coil is powered during cool-down to a very low current of 6 A. By measuring the voltage drop over the coil the resistance of the cable can be determined as function of temperature. The cool-down of the magnet was performed in the time scale of several hours (approximate rate 50 K/hour) during which the temperature difference within the coil was kept within 20 K at all times. Below the critical temperature of 93 K the voltage drops to zero indicating that the coil is now fully superconducting. The transition observed is much more gradual than for LTS coils likely due to the top of the magnet being at a different temperature than the bottom of the magnet. This gradient was more prominent due to the higher heat capacity at 93 K compared to around 10 K, the critical temperature for Nb-Ti conductors. Because the cable becomes superconducting it is not possible to determine the resistance of the matrix below the critical temperature. Therefore, in order to determine RRR, it is necessary to perform a fit. The voltage over the cable at 6 A is calculated as function of temperature, for different triple-R values, using the copper resistivity relation from CUDI [37], which is based on [38], and the composition of the cable: 15 tapes, 5.0 mm wide, consisting of 100 μm of Hastelloy and 40 μm of copper (also see Table 2). The measured voltage at temperatures of 300 K and ∼98 K (well above the transition) is compared to the calculated curves in Figure 9. The measured voltages best match a copper RRR of 20 ± 5, which is in agreement with the expected value for the HTS tape [16].

5. Training and Degradation

During the testing the quench detection was set at a threshold voltage of 20 mV with a 8 ms delay time. After detection the current extraction was performed with a 50 mΩ dump resistor and 2.5 ms IGBT switch. These parameters were selected based on numerical simulations [8], which assume adiabatic conditions and should ensure safe operation of the magnet up to 12 kA, at which point the hot-spot temperature reaches an estimated 250 K. The peak temperature at the achieved operating current of 6 kA (see Section 6) is approximately 160 K.

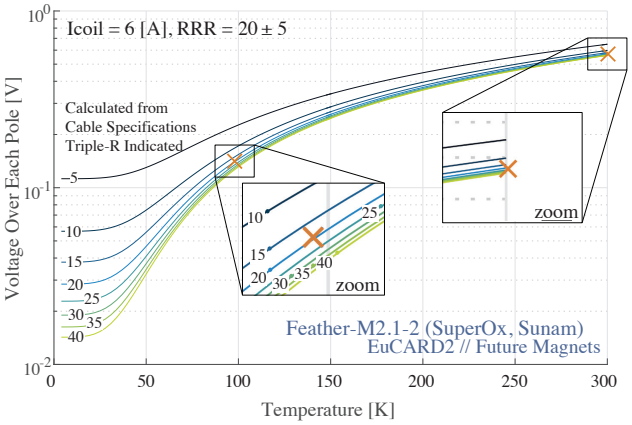

Figure 9. Determination of the RRR by fitting the calculated voltage against temperature curve against the voltage at room temperature and the voltage just before the superconducting transition, when running at 6 A. The calculation assumes similar conditions as in the coil: a 18.5 m long cable with 15 tapes, 5.5 mm wide, consisting of 100 μm of Hastelloy and 40 μm of copper. It can be seen that the RRR of the copper stabilizer is approximately 20 ± 5.

The magnet was quenched several tens of times at various temperatures and did not exhibit any training behavior. This is expected for HTS because it is many orders of magnitude more stable in terms of Minimal Quench Energies (MQE). This means that suspected training mechanisms for LTS [39], for example, cracking of the resin or small conductor movements, cannot initiate a quench in HTS. Additionally, the quenches also did not lead to any degradation of the critical current, indicating that the used protection scheme is sufficient to protect the magnet.

6. S.c. Transition and Critical Current

The Feather-M2.1-2 magnet is tested in contrast to most LTS magnets in Helium gas. This allows operation at variable temperature. At high temperatures, the critical current is very low and thus hot spot temperatures rise slowly, leaving significant time for protection. At lower temperatures during a quench, the hot-spot temperature rises rapidly leaving little time for protection. By going down in temperature in steps, the quenches remain predictable, and thus risk to the magnet is minimized.

The expected critical current of the Feather-M2.1-2 is calculated using the intersection between the load-line and the critical surface. However, because no explicit data was available on the used Sunam tape, a self-field critical current measurement was performed on a single 5.0 mm wide tape at 77 K. The critical current was determined at 300 A, making the estimated critical current of the cable approximately 4.5 kA (77 K, without self-field). This value was then used to scale the

critical surface, based on a few years old measurement data [40], to match this value. The resulting critical surface, together with the calculated load-lines of the Feather-M2.1-2 magnet, is shown in Figure 10. It can be seen that, at low magnetic fields, the critical current strongly depends on the applied magnetic field, and thus the self-field critical current is significantly higher than the critical current of the coil (even at half a tesla). This can be explained by the choice of Sunam not to include artificial pinning centers (by doping) in their tapes.

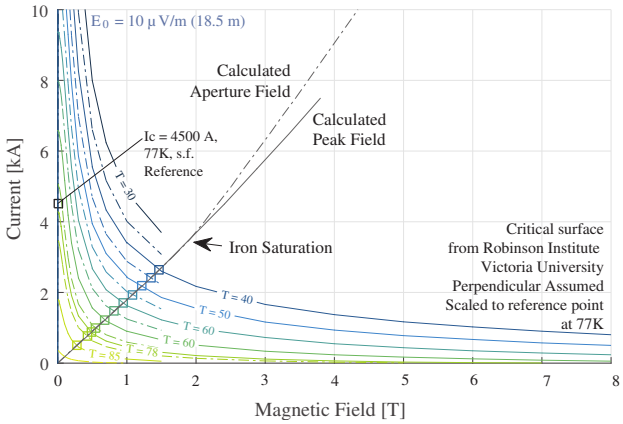

Figure 10. Prediction of the critical current using the critical surface of Sunam tape, data provided by the Robinson Institute, Victoria University, scaled to the self-field measurement at 77 K. The surface is assumed at perpendicular applied magnetic field. The intersections between the load-line of the magnet with the surface gives the critical current at each temperature.

The superconducting transition is commonly described by a power law which is given as $E = E_0[I/I_c]^N$, where I_c is the critical current, N is the so-called N-value, E is the electric field, I is the current in the conductor and E_0 is the electric field criterion to define the critical current. Classically, in LTS applications, the electric field criterion is given as $E_0 = 10\ \mu$V/m, which is the value also used in this paper. It must be noted, however, that in some other publications [41,42], reporting HTS experiments, a criterion of 100 μV/m is used. To determine the critical current the electric field in the coil is plotted against the current in a so-called EI-curve, which is defined here as the averaged electric field against the current in the coil, as opposed to en EJ-relation that describes the local behavior. This is important because it depends on the geometry of the coil: parts of the coil may have considerable less margin than other parts. As an example a measured EI-curve (using the non-inductive wire, see Section 3) is shown, at an operating temperature of 7.9 K, in Figure 11.

The critical current is then determined by fitting the power law to the data points near the transition. However, it can be seen that the magnet could be

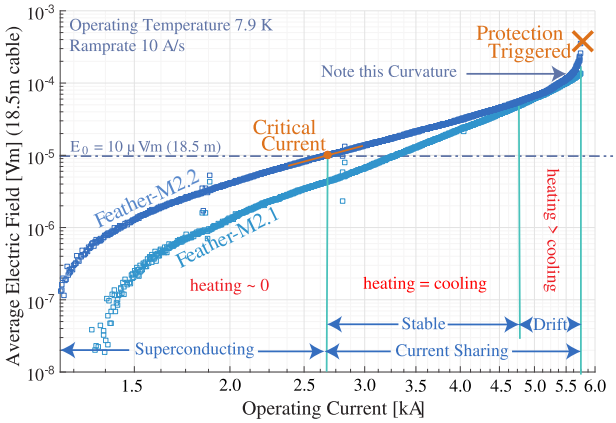

Figure 11. Measured average electric field versus current, showing the different heat-balance regimes, in the Feather-M2.1-2 at an operating temperature of 7.9 K in Helium gas.

operated far beyond the critical current, as defined by E_0. The magnet ultimately quenches at a current which is around 160% of the critical current. Beyond the critical current there is a regime in which the superconductor transitions and thus an increasing amount of current is shared between the superconductor and the matrix, causing the magnet to be partially resistive. In this regime the electric heating is counteracted by the cooling power provided by the liquid or gas. When the heating and cooling are equal, the temperature is stable and the magnet can be operated indefinitely. When the heating exceeds the cooling, the temperature drifts away slowly over minutes until eventually a quench occurs. Similar results were reported in a cryogen-free (situation similar to gas) MgB_2 coil in [43]. This type of behavior is much more apparent in HTS than in LTS due to the inherently soft transition (low N-value) and higher temperature margin. A temperature elevation, over that of the helium gas, allows a considerable amount of heat to be evacuated without triggering the typical runaway effect. This causes the region of stable current sharing to be quite extended.

It can be seen that towards higher current levels the EI-curve starts to deviate from the power law. This is likely due to the temperature continuously rising inside the coil. These assumptions are supported by a few kelvin elevation of the coil temperature with respect to the temperature of the helium gas, as measured by the regular temperature sensors located inside the copper rings (see Section 8), as well as the optical fibers located outside at the lead end of the coil. This means that measuring and mapping the local temperature rise inside the coil, when inside or near the drift region, could yield very interesting results and should be considered for future HTS magnets.

To study the current sharing regime further, the fraction of current running in the superconducting and normal conducting part of the tapes can be estimated by the solution of a parallel path model [44, 45], in which the superconductor is modeled in parallel with the resistive materials. The resulting equation, describing the distribution of current between the paths, is given as

$$\frac{E_0}{\rho}\left[\frac{I_{\rm sc}}{I_c}\right]^N - I_{sc} = I_{tot}, \qquad (1)$$

where E_0 is the electric field criterion in V/m, ρ the resistivity of the resistive part of the tape in Ω/m, I_c the critical current of the conductor in A, N is the so-called N-value, $I_{\rm sc}$ the current flowing in the superconductor and $I_{\rm tot}$ the total current flowing in the conductor, both also in A. After solving numerically for $I_{\rm sc}$, the normal conducting current can be calculated as $I_{\rm nc} = I_{\rm tot} - I_{\rm sc}$. The resulting fraction of normal conducting current, as function of total current and N-value, is presented in Figure 12. Note that the N-valueof the individual tapes should be much higher, in the range of $20 - 30$, than the N-valueof the cable, which is around 6. It can be seen that considerable amount of current, about 1%, is flowing inside the matrix at about $1.3 - 1.6$ (depending on N-value) times the critical current.

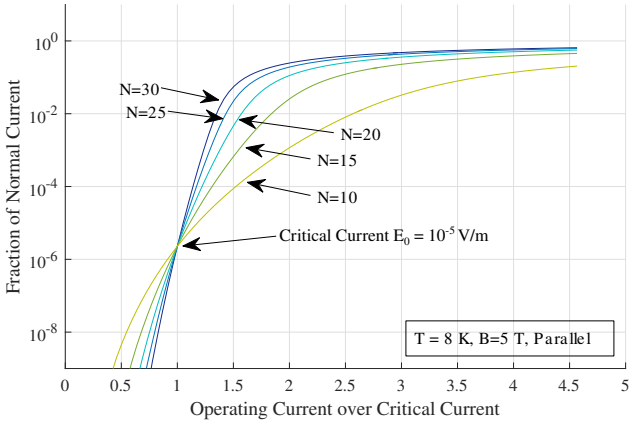

Figure 12. Calculated fraction of current flowing in the resistive part of the HTS tape as function of the operating current, which is normalized with the critical current, and N-value. A temperature of 8 K and 5 T parallel applied magnetic field are assumed.

At each temperature the magnet is ramped at a rate of 10 A/s up to its quench current. Based on the resulting EI-curves the critical current and N-valuesare determined. The first are presented, together with the quench current and predicted critical current, as function of temperature in Figure 13. Again the fully superconducting and current sharing regions are indicated. The predicted critical currents resulting from the load-line intersections with the scaled surface match well with the measured critical currents of the coil. This indicates that during coil construction no noticeable degradation has occurred. This is further confirmed by the very similar IV-characteristics between the two coils. In essence: the chances of having two coils with exactly the same degradation are very slim.

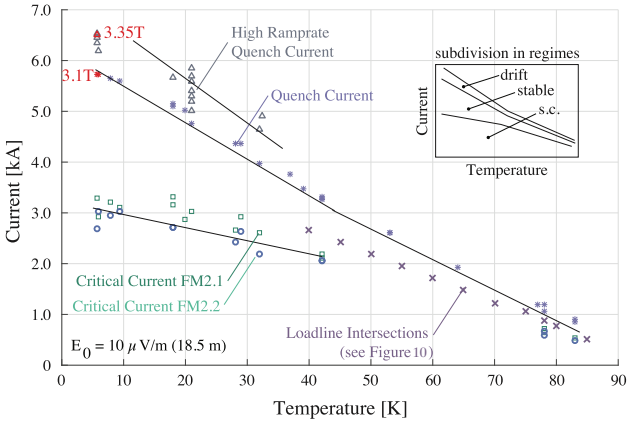

Figure 13. Measured quench and critical currents as function of temperature for the Feather-M2.1-2 (SuperOx, Sunam) high temperature superconducting magnet. Also shown, are the load-line intersections from Figure 10, which predict the critical current.

The resulting N-valuesare shown in Figure 14. The N-valueof the magnet is around 6. This is very low compared to LTS, where values of around 50 are expected, but even for HTS, which usually features N-valuesaround 20 to 30 (for single tapes) [46]. This can be explained by the current distribution between all tapes in the cable in combination with different joint resistances for each tape [47]. It can be seen that the N-valueof the coil has a slight dependence on the temperature. Towards the lower temperatures, the N-valuelikely goes down due to the reducing resistivity of the copper matrix, thereby favoring current sharing. At higher temperatures the N-valuegoes down because the distance with the critical temperature decreases. Further more accurate measurements on single tape and cable are required to confirm this observation and hypothesis.

The maximum current reached, at normal ramp-rate, was approximately 5.8 kA (also refer to Figure 13) at which the magnetic field in the aperture is 2.9 T and the peak field is 3.1 T. For reference the calculated magnetic field in the aperture along the axis is shown as function of current in Figure 15. At higher ramp-rates the quench current increases because less time is available for the coil pack to heat up in the current sharing regime. The increased coupling and hysteresis losses, causing LTS to quench at lower current at increased ramp-rates, have nearly no effect on HTS

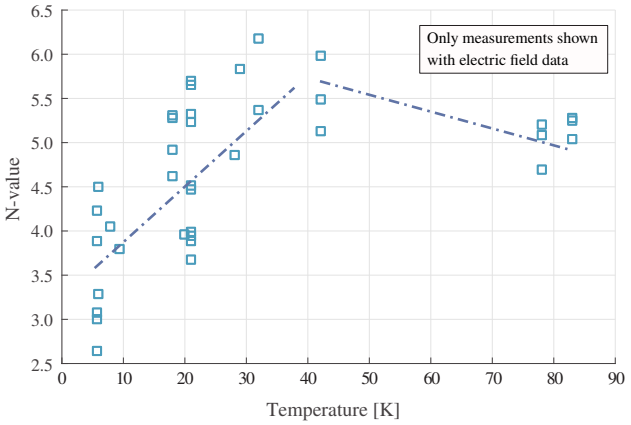

Figure 14. Measured N-valuesas function of temperature determined from the EI-curves measured on the Feather-M2.1-2 high temperature superconducting magnet.

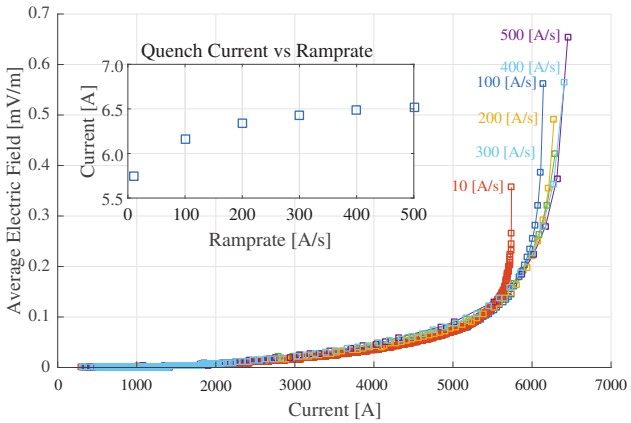

Figure 16. Measured dependence of the EI-curve on the ramp-rate at 5.7 K. It can be seen that at higher ramp-rate a higher quench current can be reached.

due to the much higher thermal margin. This causes the ramp-rate dependence of the quench current to be opposite between LTS and HTS. The quench current of Feather-M2.1-2 at an operating temperature of 5.7 K saturates at a value of about 6.5 kA (3.3 T peak field) with increased ramp-rate. The ramp-rate dependence is illustrated further in Figure 16, which shows the different EI-curves. It can be seen that at high ramp-rate the curve can reach to a higher (quench) current. The curves start to deviate at around 5.5 kA, likely also the point at which the stable regime transitions into drift. Thereby the EI-curves can possibly be used to determine this point more easily.

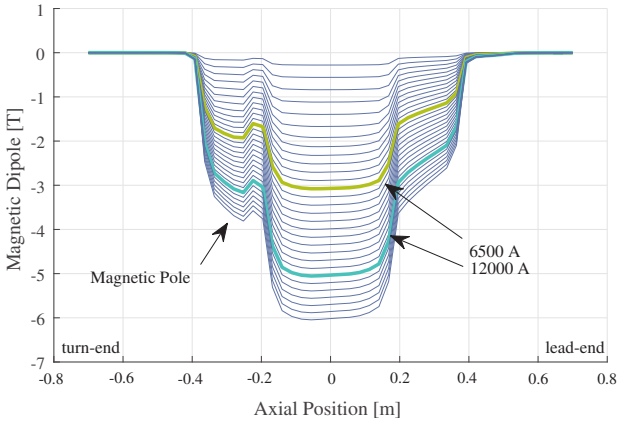

Figure 15. Calculated magnetic field along the length of the aperture for Feather-M2.1-2 as function of operating current. Highlighted is the achieved current of 6.5 kA and the design current, to be achieved with the Bruker cable, of 12 kA.

7. Detecting the Onset of a Quench

One of the main goals for the magnet test was to determine whether it is possible to detect the onset of a quench. Here it is important to differentiate between a slow and global quench and a fast local quench [8]. The first can be detected by power dissipation in the coil, which is either visible directly by a voltage drop, or indirectly by a temperature rise. The second is local, for one or several tapes, and fast, timescale 100 ms, and thus much harder to detect. This sort of quench causes a rapid sequence of current redistributions between the tapes and should therefore be visible by a signal on the pick-up coils. However, it is now believed that this type of quench may not occur at all due to the high power density required to initiate it.

During the measurement it was found that close to the quench current the voltages over the coil, as measured by the non-inductive wire, started to drift (also see Figure 11). This drift was a clear indication of an imminent quench. The reaction time however is still on the time-scale of several minutes and a small (100 A) reduction in operating current resulted in a recovery, as shown several times in the voltage recordings in Figure 17. The exponential voltage increase before a quench could in principle be quantified by taking the first and second derivative of the voltage with respect to time. If both are positive a quench is imminent.

Additionally the average electric field at which the quenches occurred always exceeded 200 μV/m, as shown in Figure 18. In essence: all observed quenches were caused by ohmic heating due to over-current and thus none of the quenches occurred unexpectedly. Limiting the average electric field at a pre-set value in combination with the detection of temperature and/or voltage drifts could be a viable method in future HTS magnets to completely avoid quenching. This is an important observation and could be extremely useful when operating at very high current densities (well) exceeding 1000 A/mm^2, potentially enabling highly

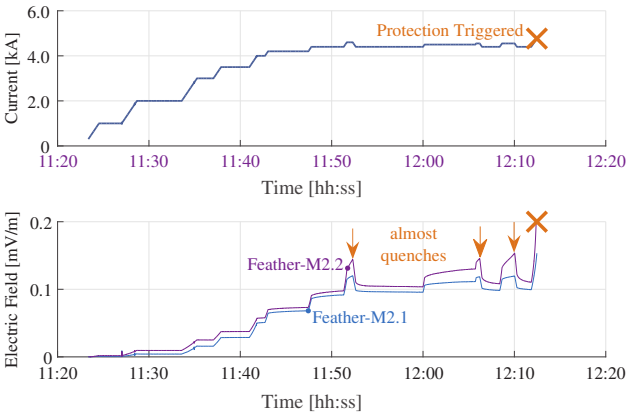

Figure 17. Measured average electric field and current as function of time demonstrating the typical behavior of an HTS magnet. It can be seen that the coil recovers three times (denoted with the arrows) by manually reducing the current just before a quench occurs. At the end of this dataset a real quench happens.

efficient (small cross-section) very high field accelerator magnets.

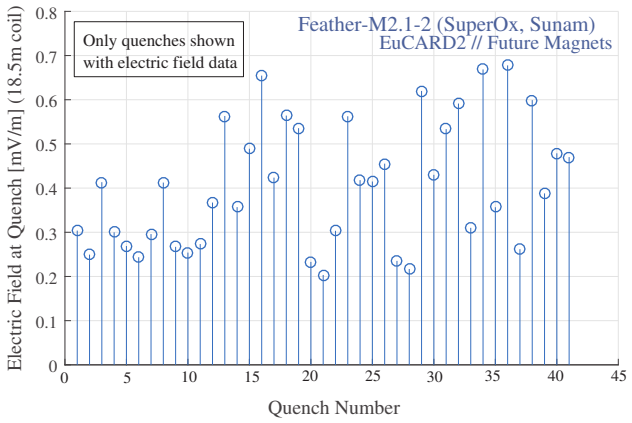

Figure 18. Measured average electric field just before the occurrence of a quench shown for a large selection of quenches in the Feather-M2.1-2 magnet. It can be seen that all quenches occurred above an average electric field of 200 μV/m.

The pick-up coils did not see any signals prior to the fast discharge over the dump resistor. This could either be caused by the high noise floor of the used detection system (10 mV, 1 kHz) or by the absence of any current distribution during the quenches. The latter is likely the case since all quenches occurred at high average electric field. At this point all tapes inside the cable are partially resistive. The current distribution between the tapes is dominated by this resistance and thus all tapes are filled with current. An increase of the transport current or temperature more would quench all tapes simultaneously and thus no significant current redistribution would occur. A cable with a higher engineering current density may show much more redistribution of the current. Further experiments are expected to verify this.

8. Quench Protection and Copper Ring

To reduce the decay time of the current, when extracting with a dump resistor a copper ICED ring was added around the coil pack (also see Section 2). When the dump resistor is switched into the circuit, part of the current is transferred inductively into the ring, effectively extracting about 40% of the energy from the magnet, a concept often effectively applied to large solenoidal detector magnets. This could prove useful for future HTS magnets, where the extraction times limit the maximum current density and thus the efficiency of the magnet. Additional advantages are that the copper around the coil also provides extra cooling, through thermal conduction, and additional heat capacity, corresponding to reaction time, to the coil pack. Note that if an imminent quench can be reliably detected tens of seconds ahead of time, fast extraction and thus this type of system will not be necessary. Additionally, the copper rings could have a significant impact on the field quality due to induced currents during ramping and should be studied with care [22, 32].

Figure 19 presents the modeled and measured current decay of the Feather-M2.1-2 magnet. In the model the copper ring is included through a mutual inductance matrix assuming a coupling coefficient of 0.8. Additionally also the exponential LR-decay without copper ring is shown. It can be seen that the decay matches significantly better with the model including the copper ring. The temperature of the copper ring before and after a quench at 5.5 kA with an operating temperature of 8 K, is shown in Figure 20. The temperature rise before the quench is caused by the heating of the coil pack during the drift. After the quench the temperature rises rapidly up to 30 K due to the power dissipation in the ring. The temperature rise agrees well with numerical prediction. Based on the measured current decay, compared to numerical simulations, and the temperature rise of the ring, during extraction, it can be concluded that this concept is working as expected.

9. Joint Resistances

A new joint system named Fin-Block [48] was used in the Feather-M2 magnet for the first time. During the testing the joints did not show any significant temperature rise and were not limiting the current, like they were in the Feather-M0.4 test [19]. Sub-cooling of the joints, as done in Feather-M0.4, was not necessary. The joint resistances are determined by linear fitting

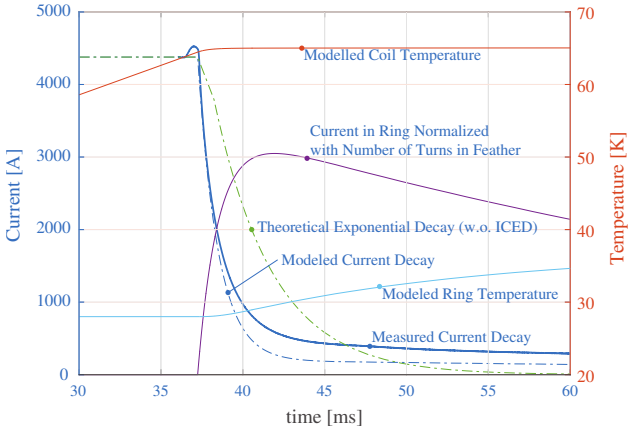

Figure 19. Comparison between the modeled and measured current decay after the switching of the dump resistor. It can be seen that the model including the copper ring is in good agreement with the measured data, while the theoretical exponential decay (not including the ring) fails to predict the behavior correctly.

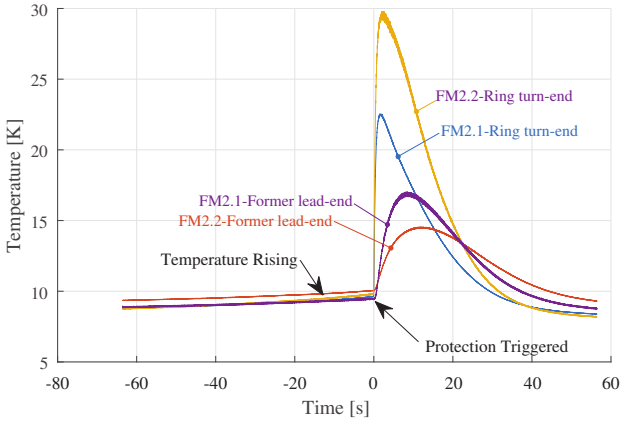

Figure 20. Measured temperature inside the copper rings and formers of Feather-M2.1-2 against time before and after the quench, which occurs at 0 seconds. It can be seen that before the quench, the temperature drifts away, after the quench a spike indicates that part of the energy has effectively been extracted by the copper rings.

of the voltages against the current. The resulting values are presented as function of temperature in Figure 21. Joint resistances are all below 150 nΩ at 77 K and are below 19 nΩ at 10 K. This difference is caused by the resistivity of the copper, used for the various parts of the joint, which is strongly dependent on the temperature. Although the joints were no longer limiting the current, it must be noted that the Fin-Block configuration was much more difficult to handle during magnet assembly and in the test station than conventional joints due to its higher weight.

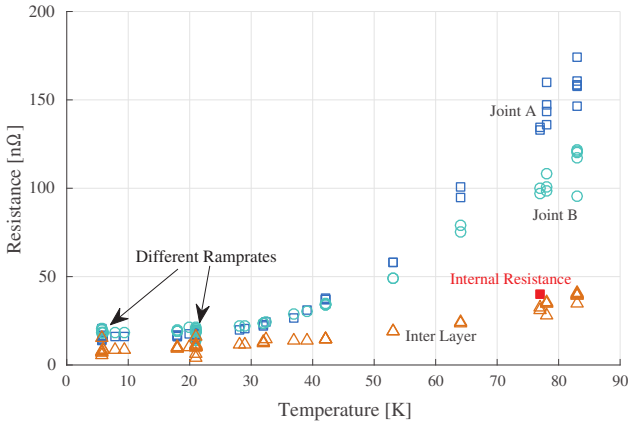

Figure 21. Joint resistances as function of temperature resulting from linear fitting of the measured voltages over the joints against the operating current of the magnet. See the electrical diagram in Figure 7 for the location of the joints.

10. Conclusion

The full-scale coil Feather-M2.1-2 (SuperOx, Sunam) was successfully tested at variable temperature in Helium gas up to a magnetic field of 3.1 T in the aperture and a magnetic peak field of 3.3 T on the conductor, which was reached at a temperature of 5.7 K and a current of 6.5 kA. These results demonstrate that with the performance of the next cables of EuCARD2 (tape processed by Bruker and cable assembled by KIT), which are presently being wound into the next coils Feather-M2.3-4, the EUCARD2 requirement of 5 T should easily be achieved.

The non-inductive backing wire has about one-third of the noise level than the differential signal between the two poles of the magnet. This type of measurement is useful for analysis of the behavior of the coil and should be considered for all magnets. A large, approximately factor 1.6, difference was found between the fitted critical current, at the traditional electric field criterion of 10 μV/m, and the quench current. Beyond the critical current an increasing amount of current is shared with the resistive part of the conductor, causing the magnet to become partially resistive, resulting in heating. The current sharing can be subdivided further in a stable zone and a drift zone. In the stable zone the heat balance between heating and cooling result in a stable temperature, and thus the magnet can be operated indefinitely. In the drift zone the heating exceeds the cooling, causing the temperature in the coil to rise over a time scale of minutes, eventually leading to a quench.

The critical current of the coil is compared to experimental Sunam critical current data, appropriately scaled using a 77 K measurement. The critical cur-

rents resulting from the load-line intersections match well with the measured critical currents of the coil. This indicates that during coil construction no degradation has occurred in vital locations. In addition, both coils have very similar V-I characteristics, which further confirms that no degradation of the critical current occurred during construction.

The magnet was quenched several tens of times and did not exhibit any training behavior. This means that suspected training mechanisms for LTS, like cracking of the resin, do not initiate a quench in HTS. Also no degradation of the critical current was observed indicating that the protection scheme was sufficient. The onsets of the quenches were clearly visible by an exponential increase of the voltage many seconds in advance. In addition a temperature increase was observed both on classical temperature probes and on optical fibers. When the current is ramped down by a small amount (only 100 A) just before the quench, the magnet is able to recover.

References

[1] L. Rossi et al. The EuCARD-2 Future Magnets project: the European collaboration for accelerator quality HTS magnets. *IEEE Transactions on Applied Superconductivity*, 25(3), August 2014.

[2] G. Kirby, L. Rossi, M. Bajko, et al. Status of the Demonstrator Magnets for the EuCARD-2 Future Magnets Project. *IEEE Transactions on Applied Superconductivity*, 26(3), April 2016.

[3] P. Ferracin, M. Devaux, M. Durante, et al. Development of the EuCARD Nb_3Sn Dipole Magnet FRESCA2. *IEEE Transactions on Applied Superconductivity*, 23(3), June 2013.

[4] E. Rochepault, N. Bourcey, P. Ferracin, et al. Mechanical Analysis of the FRESCA2 Dipole During Preload, Cool-Down, and Powering. *IEEE Transactions on Applied Superconductivity*, 28(3), April 2018.

[5] G. Willering, C. Petrone, M. Bajko, et al. Cold Powering Tests and Protection Studies of the FRESCA2 100 mm Bore Nb3Sn Block-Coil Magnet. *IEEE Transactions on Applied Superconductivity*, PP(99), 2018.

[6] A. Koski and S. L. Wipf. Computational design study for an accelerator dipole in the range of 15-20 T. *IEEE Transactions on Magnetics*, 32(4):2159–2162, Jul 1996.

[7] J. van Nugteren, G. Kirby, G. de Rijk, et al. Study of a 5 T Research Dipole Insert-Magnet Using an Anisotropic ReBCO Roebel Cable. *IEEE Transactions on Applied Superconductivity*, 25(3):1–5, June 2015. © 2015 IEEE. Figures and Tables Adapted, with permission.

[8] J. van Nugteren. *High Temperature Superconductor Accelerator Magnets*. PhD thesis, University of Twente, 2016.

[9] L. Roebel. Electrical conductor. US Patent 1,144,252, June 1915.

[10] C. Albrecht, P. Massek, and P. Kummeth. Fully transposed high tc composite superconductor, method for producing the same and its use. WO 2001059909 A1, August 2001. Siemens Aktiengesellschaft.

[11] N.J. Long, R.A. Badcock, C. Bumby, and Z. Jiang. *Superconductivity: Recent Developments and New Production Technologies*, chapter Production and Characterisation of HTS Roebel cable. Nova publishers, 2012.

[12] W. Goldacker, A. Frank, R. Heller, et al. ROEBEL Assembled Coated Conductors (RACC): Preparation, Properties and Progress. *IEEE Transactions on Applied Superconductivity*, 17(2):3398–3401, June 2007.

[13] J. Fleiter, A. Ballarino, W. Goldacker, and A. Kario. Characterization of Roebel cables for potential use in high-field magnets. *IEEE Transactions on Applied Superconductivity*, 25(3), August 2014.

[14] website: http://www.superox.ru/en/. visited: 17-July-2017.

[15] website: http://i-sunam.com/. visited: 17-July-2017.

[16] C. Senatore, C. Barth, M. Bonura, et al. Field and temperature scaling of the critical current density in commercial REBCO coated conductors. *Superconductor Science and Technology*, 29(1), 2016.

[17] website: https://www.bruker.com/. visited: 17-July-2017.

[18] website: https://www.itep.kit.edu/. visited: 17-July-2017.

[19] G. Kirby, J. van Nugteren, H. Bajas, et al. First Cold Powering Test of REBCO Roebel Wound Coil for the EuCARD2 Future Magnet Development Project. *IEEE Transactions on Applied Superconductivity*, 27(4), June 2017.

[20] W. Barletta, M. Battaglia, M. Klute, et al. Future hadron colliders: From physics perspectives to technology R&D. *Nuclear Instruments and Methods*, 764:352–368, 2014.

[21] D. Schoerling, H. Bajas, M. Bajko, et al. Strategy for Superconducting Magnet Development for a Future Hadron-Hadron Circular Collider at CERN. *Proceedings of science*, 2015.

[22] C. Petrone, J. van Nugteren, H. Bajas, et al. Measurement and Analysis of the Dynamic Effects in an HTS Dipole Magnet. *IEEE Transactions on Applied Superconductivity*, PP(99), 2018.

[23] V. Lombardo, E. Barzi, D. Turrioni, et al. Fabrication, qualification and test of high Jc Roebel $YBa_2Cu_3O_{7-\delta}$ coated conductor cable for HEP magnets. *IEEE Transactions on Applied Superconductivity*, 21:2331–2334, 2011.

[24] D. Uglietti, R. Wesche, and P. Bruzzone. Effect of transverse load on the critical current of a coated conductor Roebel cable. *Superconductor Science and Technology*, 26(7), 2013.

[25] T. Takematsu, R. Hu, T. Takao, et al. Degradation of the performance of a YBCO-coated conductor double pancake coil due to epoxy impregnation. *Physica C: Superconductivity*, 470(1718):674–677, 2010.

[26] C. Barth, N. Bagrets, K-P Weiss, et al. Degradation free epoxy impregnation of REBCO coils and cables. *Superconductor Science and Technology*, 26(5), 2013.

[27] Composite Technology Development. *CTD-101K, Epoxy Resin System*, 2003. available at: http://www.CTD-materials.com.

[28] S. Otten. Transverse Pressure Dependence of the Critical Current in Epoxy Impregnated ReBCO Roebel Cables. Master's thesis, University of Twente, October 2014.

[29] S Otten, M Dhallé, P Gao, W Wessel, A Kario, A Kling, and W Goldacker. Enhancement of the transverse stress tolerance of REBCO Roebel cables by epoxy impregnation. *Superconductor Science and Technology*, 28(6), 2015.

[30] M. Gupta, R. Anerella, A. Ghosh, et al. High Field HTS Solenoid for a Muon ColliderDemonstrations, Challenges, and Strategies. *IEEE Transactions on Applied Superconductivity*, 24(3), June 2014.

[31] G. Kirby, J. van Nugteren, A. Ballarino, et al. Accelerator Quality HTS Dipole Magnet Demonstrator Designs for the EuCARD-2, 5 T, 40 mm Clear Aperture Magnet. *IEEE Transactions on Applied Superconductivity*, 25(3), December 2014.

[32] J. Murtomaki, J. van Nugteren, G. Kirby, et al. Inductively Coupled Energy Dissipater (ICED) for Future High Field Accelerator Magnets. Technical report, CERN, 2016.

[33] J. Ruuskanen, A. Stenvall, J. van Nugteren, and V. Lahtinen. Optimization of an E^3SPreSSO Energy-Extraction System for High-Field Superconducting Magnets. *IEEE Transactions on Applied Superconductivity*, 28(3):1–5, April 2018.

[34] G. Willering, M. Bajko, F. Borgnolutti, et al. Fast Cycled Magnet Demonstrator Program at CERN: Instrumentation and Measurement Campaign. *IEEE Transactions on Applied Superconductivity*, 24(3), June 2014.

[35] F. Hunte, H. Song, and J. Schwartz. Fiber Bragg Optical Sensors for YBCO Applications. In *Proceedings of the 9th international particle accelerator conference*, pages 3675–3677, 2009.

[36] A. Chiuchiolo et al. Fiber Bragg Grating Cryosensors for Superconducting Accelerator Magnets. *IEEE Photonics Journal*, 6(6):1–10, December 2014.

[37] CERN. *CUDI: Users Manual*, 1992.

[38] M.S. McAshan. MIITs integrals for copper and for Nb-46.5wt%Ti. Technical report, SCC Laboratory, February 1988.

[39] M. Wilson. *Superconducting Magnets*, chapter 5. Clarendon Press Oxford, Great Clarendon Street, Oxford OX2 6DP, 1983. ISBN 0-19-854810-9.

[40] S. Wimbush and N. Strickland. A Public Database of High-Temperature Superconductor Critical Current Data. *IEEE Transactions on Applied Superconductivity*, 27(4):1–5, June 2017.

[41] D. Hu, M.D. Ainslie, M.J. Raine, et al. Modeling and Comparison of In-Field Critical Current Density Anisotropy in High-Temperature Superconducting (HTS) Coated Conductors. *IEEE Transactions on Applied Superconductivity*, 26(3), April 2016.

[42] F. Grilli, E. Pardo, A. Stenvall, et al. Computation of Losses in HTS Under the Action of Varying Magnetic Fields and Currents. *IEEE Transactions on Applied Superconductivity*, 24(1):78–110, 2014.

[43] A. Stenvall, I. Hiltunen, A. Korpela, et al. A checklist for designers of cryogen-free MgB_2 coils. *Superconductor Science and Technology*, 20(4):386–391, 2007.

[44] Z. J. J. Stekly and J. L. Zar. Stable Superconducting Coils. *IEEE Transactions on Nuclear Science*, 12:367–372, June 1965.

[45] S. Russenschuck. *Field Computation for Accelerator Magnets*. Book, Wiley, 2010.

[46] A.K. Ghosh. V–I transition and n-value of multifilamentary LTS and HTS wires and cables. *Physica. C, Superconductivity*, 9(6), 2004.

[47] G. Willering, D. van der Laan, H. Weijers, et al. Effect of variations in terminal contact resistances on the current distribution in high-temperature superconducting cables. *Superconductor Science and Technology*, 28(3), January 2015.

[48] J. Murtomäki, G. Kirby, J. van Nugteren, et al. 10 kA Joints for HTS Roebel Cables. *IEEE Transactions on Applied Superconductivity*, PP(99), 2018.